Communication

S-Band Full-Metal Circularly Polarized Cavity-Backed Slot Antenna With Wide Bandwidth and Wide Beamwidth

Rui-Sen Chen, Lei Zhu, Sai-Wai Wong, Jing-Yu Lin, Yin Li, Long Zhang, and Yejun He

***Abstract*— In this communication, an *S*-band wide-bandwidth and wide-beamwidth full-metal circularly polarized (CP) cavity-backed slot antenna is proposed. A pair of triangular prisms placed at the corners of the cavity is introduced to produce TE_{101} and TE_{011} modes with orthogonal electric fields. These two modes are used to achieve the CP radiation and radiate the energy through a single-circular slot. By simultaneously varying the prisms' size and slot radius, the axial ratio (AR) bandwidth (ARBW) improves. The ARBW is further improved by replacing the circular slot with an elliptical slot. As a result, the ARBW increases from 1.0% to 10.3% without complicating the antenna structure and without enlarging the antenna size. Besides, the antenna still operates at two degenerate modes to introduce stable radiation gain and pattern. In addition, the proposed CP slot antenna features a wide ARBW. The final measurement shows that the proposed CP antenna can achieve a 9.5% bandwidth, a stable gain of 7.65 dBic ± 0.15 dBic, and higher than 140° ARBWs in a wide frequency range. The peak total radiation efficiency and aperture efficiency are about 97% and 91%, respectively.**

***Index Terms*— Cavity-backed slot antenna (CBSA), circularly polarized (CP), full metal, high-efficiency, wide axial ratio (AR) beamwidth, wideband.**

I. Introduction

Cavity-backed slot antennas (CBSAs) possess attractive features such as unidirectional radiation pattern, high gain, and high radiation efficiency, which have been comprehensively demonstrated in open literatures [1]–[8]. CBSAs designed using SIW cavity [1]–[3] have low profile and low cost, but relatively low efficiency caused by the dielectric loss of the substrate when compared to full-metal CBSAs [4]–[8]. Besides, full-metal slot antenna has a high power-handling capacity, which is highly demanded in high-power and long-distance communication systems, such as satellite communication and radar communication.

Circularly polarized (CP) antennas can reduce polarization mismatch and multipath interference and are widely applied in positioning, navigation, satellite, and radar wireless communication systems. So far a lot of CP slot antennas using backed cavity have been reported in the literatures which were implemented by SIW cavity [9]–[13] and metal cavity [14]–[19]. The single-element CP slot antennas or their subarrays with small number of elements, based on the degenerate modes without the utilization of power dividing network, usually suffered from a narrow axial ratio (AR) bandwidth (ARBW), thus limiting their applications [9]–[11], [14], [15]. In [9], the CP antenna based on two orthogonal SIW cavity modes TE_{120} and TE_{210} and a cross slot has a narrow ARBW of 0.8%. In [15], the TE_{101} and TE_{011} cavity modes were used to design the CP slot antenna with the perturbation of a cross slot (or two pairs of parallel slots), while it likewise had a narrow ARBW of 1%. Thus, wide ARBW could often be obtained in the design of slot array [12], [13], [16]–[19], where the feeding network of the slot array brings in the wideband characteristic.

Another important property of the CP antennas is that a wide AR beamwidth is often needed to enlarge the coverage area. For instance, the global positioning system (GPS) requires a 3 dB beamwidth of 120° to receive as many satellite signals as possible from any place on earth. However, the CP CBSAs with wide AR beamwidth had not been intensively reported so far. In [11], a CP SIW slot antenna with 70° AR beamwidth was presented. In [20], the high-order SIW modes were used to design a 4×4 CP slot array, which had an AR beamwidth of less than 70°. In [21], a metasurface-based CP SIW slot array can achieve an AR beamwidth of 57°. Nevertheless, the AR beamwidths of these CP slot antennas were only reportedly obtained at the center frequencies, in addition to their narrow ARBWs. Besides, on the one hand, these antennas suffered from a relatively narrow AR beamwidth and a narrow ARBW. On the other hand, those slot arrays can obtain a wideband ARBW [12], [13], [16]–[19], but they suffer from narrow radiation beamwidth and AR beamwidth due to the large antenna size. Thus, in general, wide ARBW and wide AR beamwidth cannot be simultaneously obtained in the reported CP slot antennas.

In this communication, we would like to focus our attention on the design of a CP slot antenna with enhanced ARBW and wide AR beamwidth. Two triangular prisms are introduced at diagonal corners to perturb the TE_{101}, so as to generate a new TE_{011} mode, which are combined to achieve CP radiation. This diagonal perturbation had been reported in [22]–[24] to design CP dielectric resonator antennas, where the enhancement of ARBW was not discussed. The triangular prisms in proposed antenna are purposely used to enhance the ARBW in cooperation with the radiation slot. The magnitude ratio and phase difference between the two orthogonal electric field components under the effect of prism and slot are studied to understand the improvement in ARBW. In addition, by replacing the circular radiation slot with an elliptic slot, the ARBW is further widened. As a result, the ARBW is increased from 1.0% to 10.3% without introducing other antenna structures and without enlarging the antenna's size. This antenna still operates at TE_{101} and TE_{011} cavity modes, resulting in the realization of a stable radiation gain and radiation pattern. The two orthogonal electric field components have similar magnitudes and nearly 90° phase difference in wide

Manuscript received August 19, 2020; revised January 1, 2021; accepted January 27, 2021. Date of publication March 1, 2021; date of current version September 3, 2021. This work was supported in part by the National Natural Science Foundation of China under Grant 62071306; in part by the Shenzhen Science and Technology Programs under Grant JCYJ20180305124543176 and Grant JCYJ20190728151457763; in part by the Natural Science Foundation of Guangdong Province under Grant 2018A030313481; and in part by the Shenzhen University Research Startup Project of New Staff under Grant 860-000002110311. *(Corresponding author: Sai-Wai Wong.)*

Rui-Sen Chen is with the College of Electronics and Information Engineering, Shenzhen University, Shenzhen 518060, China, and also with the Department of Electrical and Computer Engineering, Faculty of Science and Technology, University of Macau, Macau 999078, China.

Lei Zhu is with the Department of Electrical and Computer Engineering, Faculty of Science and Technology, University of Macau, Macau 999078, China.

Sai-Wai Wong, Yin Li, Long Zhang, and Yejun He are with the College of Electronics and Information Engineering, Shenzhen University, Shenzhen 518060, China (e-mail: wongsaiwai@ieee.org).

Jing-Yu Lin is with the School of Electrical and Data Engineering, University of Technology Sydney, Ultimo, NSW 2007, Australia.

Color versions of one or more figures in this communication are available at https://doi.org/10.1109/TAP.2021.3061116.

Digital Object Identifier 10.1109/TAP.2021.3061116

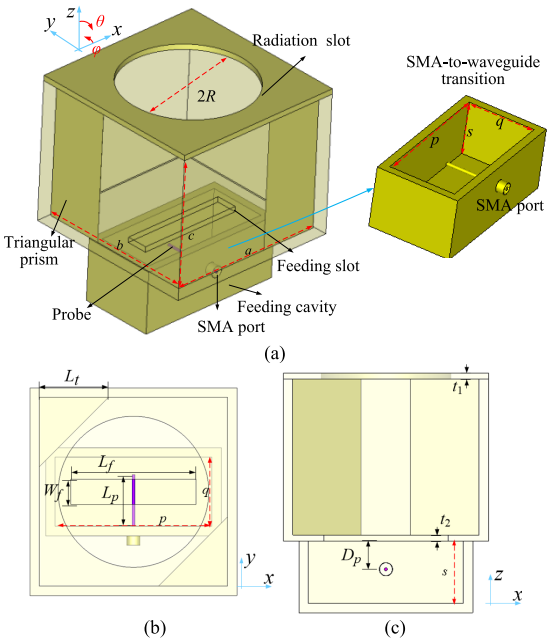

Fig. 1. Proposed CP cavity-backed antenna. (a) 3-D view. (b) Top view at *xy*-plane. (c) Side view at *xz*-plane.

angle range, thus obtaining a wide AR beamwidth. In this context, both wide ARBW and wide AR beamwidth are well achieved in the proposed wideband CP slot antenna. Finally, an antenna prototype is designed at *S*-band (around 3.5 GHz). The measurement shows that the proposed antenna has 9.5% ARBW and 140° AR beamwidth, and the realized gain and radiation pattern are stable over the operating band.

II. Operation Principle and Design

A. Realization of Circular Polarization

Fig. 1 shows the configuration of the proposed CBSA, which is composed of a resonant cavity with two loaded triangular prisms, a radiation slot, a feeding cavity, a feeding slot, and a feeding probe. The feeding cavity and feeding probe are combined to form an SMA-to-waveguide transition, which is integrated into the antenna structure to excite the cavity modes through the feeding slot. A pair of triangular prisms is placed at the diagonal corners of the cavity, and the conventional two crossed slots are replaced by a single circular radiation slot.

In this antenna, the cavity modes TE_{101} and TE_{011} are used to obtain the CP radiation. Their original resonant frequencies are calculated using (1a) and (1b), respectively. The v represents the light speed in free space and a, b, and c are the side lengths of the cavity. As TE_{101} and TE_{011} modes are considered as a pair of degenerate modes and are potentially utilized to design CP antenna under proper perturbation, and their original frequencies are set identical, i.e., $a = b$

$$f_{TE_{101}} = \frac{v}{2}\sqrt{\left(\frac{1}{a}\right)^2 + \left(\frac{1}{c}\right)^2} \tag{1a}$$

$$f_{TE_{011}} = \frac{v}{2}\sqrt{\left(\frac{1}{b}\right)^2 + \left(\frac{1}{c}\right)^2}. \tag{1b}$$

The triangular prism produces the perturbation on the cavity mode TE_{101} so as to generate a new cavity mode TE_{011}. These two modes have orthogonal field distributions and they can be applied to achieve CP radiation under a proper perturbation. Fig. 2 shows the simulated $|S_{11}|$ and AR without prism ($L_t = 0$ mm) and with prism

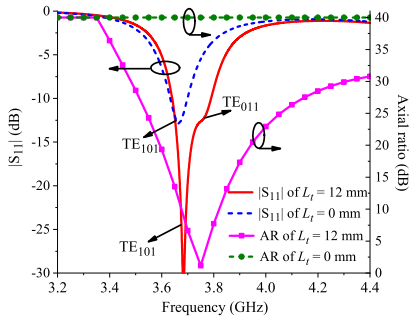

Fig. 2. Simulated results with and without metal prisms.

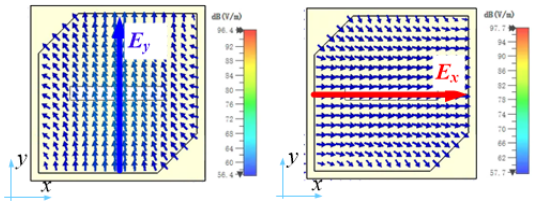

Fig. 3. Electric field distributions at (a) 3.68 GHz and (b) 3.78 GHz.

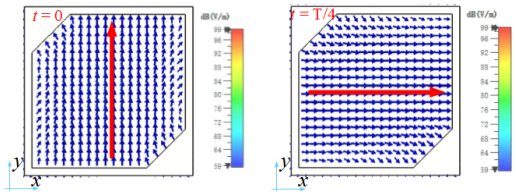

Fig. 4. Electric field distributions at 3.75 GHz at different time instances. (a) $t = 0$. (b) $t = T/4$.

TABLE I
Dimensions of Narrowband CP Slot Antenna

Symbol	a	b	c	p	q	s	R	L_t	L_f	W_f	D_p	L_p	t_1	t_2
Value (mm)	60	60	50	50	22	20	17	12	36	8	6	18	2	2

($L_t = 12$ mm). It can be seen that only a single mode (TE_{101} mode) is excited when $L_t = 0$ mm. The frequency discrepancy between the simulated one (3.68 GHz) and calculated one (3.93 GHz) is due to the loading effect of the feeding slot and radiation slot. With the effect of the prisms ($L_t = 12$ mm), one more mode, i.e., TE_{011} mode, is generated. It can be seen that the TE_{101} mode still resonates at its original frequency of 3.68 GHz, while the TE_{011} mode resonates at a higher frequency of 3.78 GHz. Their electric field distributions are shown in Fig. 3(a) and (b), respectively. These two modes produce a CP radiation of around 3.75 GHz since they have same magnitude and 90° phase difference, as shown in Fig. 4. The ARBW in Fig. 2 attains about 1.0%. The dimensions of the narrowband CP slot antenna is provided in Table I. The cavity size in terms of free-space wavelength is $0.75\lambda_0 \times 0.75\lambda_0 \times 0.62\lambda_0$.

As derived from (1), the cavity size can influence the resonant frequencies of the cavity modes and consequently influence the antenna's operating frequency in terms of impedance band and AR band. To understand that, the effect of the cavity size on the antenna is shown in Fig. 5. It can be seen that the increasing size of resonant cavity introduces a decreasing antenna's operating frequency, which is kept consistent with the derived results from (1).

B. Improvement in ARBW

Then let us discuss the improvement in ARBW. It is noted that the ARBW can be improved under the operation of the two degenerate

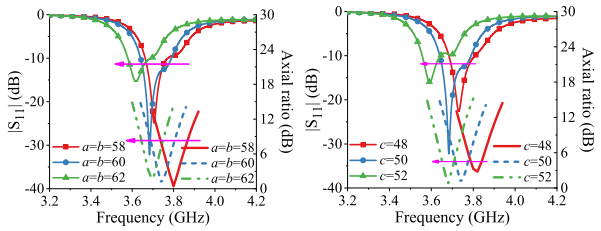

Fig. 5. Parametric study of the cavity size. (a) Effect of a and b. (b) Effect of c.

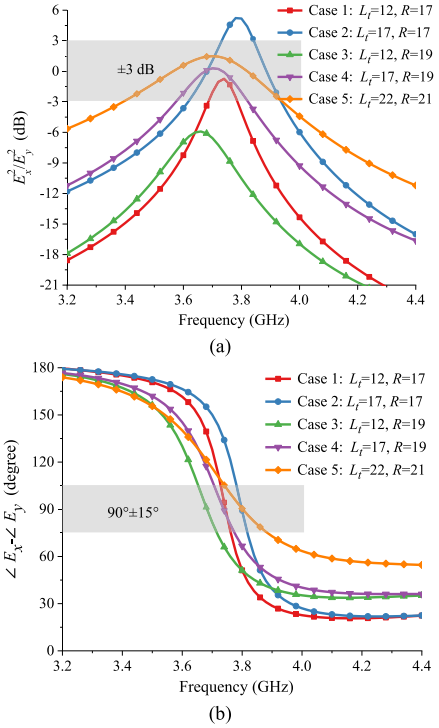

Fig. 6. Magnitude ratio and phase difference of E_x and E_y under different conditions of prisms' size and slot's size. (a) Magnitude ratio. (b) Phase difference.

modes and a single-antenna element without introducing extra feeding networks or coupling structures.

The ideal CP radiation with AR $=$ 1 is obtained under the conditions of $E_x = E_y$ and $\angle E_x - \angle E_y = 90°$, where E_x and E_y are the two electric field components for obtaining CP wave [25]. To obtain a wide ARBW, the following two requirements should be satisfied.

1) The magnitude ratio E_x/E_y is approximately equal to 1 in a wide frequency range.
2) The phase difference is approximately equal to 90° in the same frequency range of requirement 1).

In this CP slot antenna, the main perturbation is contributed by the prisms and the radiation slot. Their effects on the magnitude ratio and phase difference between E_x and E_y are shown in Fig. 6. Fig. 6(a) indicates that the individual increase in L_t (Case 1 to case 2) and the individual increase in R (Case 1 to case 3) cannot improve the ARBW, as they both cause the magnitude ratio beyond 3 dB. While the simultaneous increase in L_t and R (Case 1 to case 4 to case 5) can widen the bandwidth with a magnitude ratio of around ±3 dB. Fig. 6(b) also indicates that the simultaneous increase in L_t and R can widen the bandwidth with a phase difference of around 90° ($90° \pm 15°$). Thus, the simultaneous increase in L_t and R can indeed

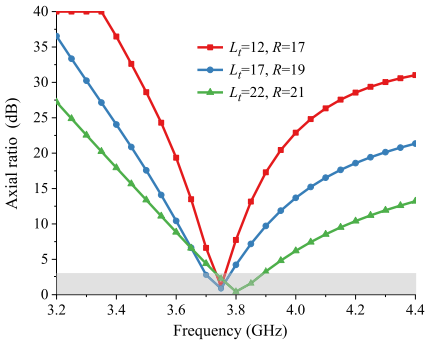

Fig. 7. Simulated AR under conditions of varying prism and slot sizes.

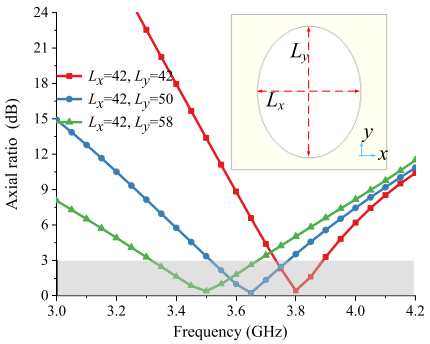

Fig. 8. Enhanced ARBW by replacing the circular radiation slot with the elliptical radiation slot.

satisfy the requirements of 1) and 2), which consequently widen the ARBW.

Fig. 7 shows the simulated AR under the condition of varying prism and slot sizes. It can be seen that when the L_t and R simultaneously increase, the ARBW increases. The 3 dB ARBW covers a range from 3.73 to 3.9 GHz with a bandwidth of 4.5% under $L_t = 22$ and $R = 21$, which is wider than the original one of 1.0%.

The previous analysis regarding the improvement in ARBW is conducted based on a circular radiation slot. To further enhance the ARBW, the circular radiation slot is replaced by an elliptic radiation slot, as shown in Fig. 8. The elliptic slot has different diameters in x-axis and y-axis, which produces different perturbations on two degenerate modes, and has the potential to widen the ARBW. Fig. 8 shows the effect of increasing the diameter in y-axis (L_y) while the diameter in x-axis (L_x) is kept unchanged. It can be seen that when L_y is increased from 42 to 58 mm, the ARBW increases from 4.5% to 10.3%. For a clear insight into the operating mechanism, the electric field orientations on the radiation slots at different time instances and different frequencies are given in Fig. 9. It can be seen that the electric fields at 3.4, 3.5, and 3.6 GHz all have a 90° phase difference between adjacent quarter time instances.

C. Analysis of AR Beamwidth

Then the performance of AR beamwidth is presented. Fig. 10 shows the magnitude ratio and phase difference in E_x and E_y at xz-plane and yz-plane as a function of theta. The magnitude ratio at xz-plane in the angle range of $-74° \sim +74°$ is within ±2 dB, and that the angle range of $-80° \sim +80°$ is within ±3 dB, while the phase difference ranges from 90° to 100° in the angle range of $-85° \sim +85°$. The magnitude ratio at yz-plane in the angle range of $-70° \sim +70°$ is within ±2 dB, and that in the angle range of $-82° \sim +82°$ is within ±3 dB, while the phase difference is ranged from 89° to 94° in the angle range of $-86° \sim +86°$. Thus, it can be understood from Fig. 11 that the proposed CP antenna can widen

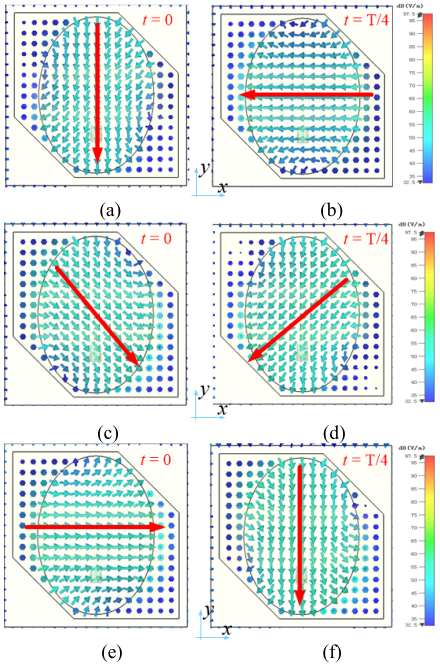

Fig. 9. Electric field orientations within radiation slot at time instances of $t = 0$ and $t = T/4$. (a) and (b) 3.4 GHz. (c) and (d) 3.5 GHz. (e) and (f) 3.6 GHz.

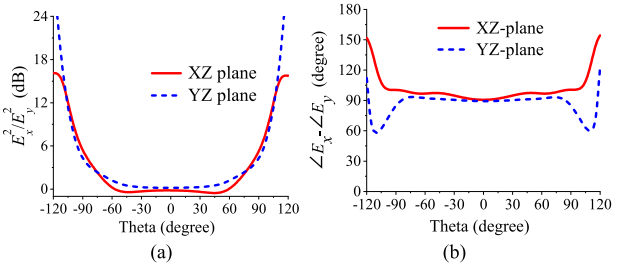

Fig. 10. (a) Magnitude ratio and (b) phase difference in E_x and E_y at xz-plane and yz-plane at 3.5 GHz with function of theta.

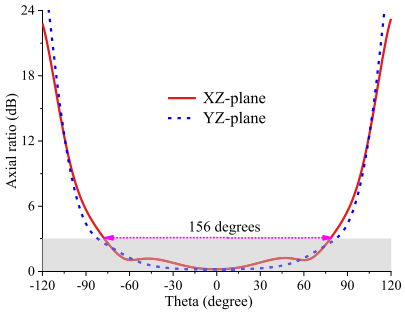

Fig. 11. Simulated AR beamwidth of the proposed CP slot antenna at 3.5 GHz.

the concerned AR beamwidth. The 3 dB AR beamwidths at xz-plane and yz-plane are 156° and 160°, respectively. The inherent factors of wide AR beamwidth are as follows.

1) The single resonant cavity introduces a relatively small antenna size, which can maintain a wide radiation beamwidth.
2) The backed cavity serves as a finite ground plane, which can reshape the radiation pattern at E-plane and H-plane, and then makes these two radiation patterns more similar to each other.

D. Impedance Matching

After determining the radiation performance, the input impedance of the antenna is also determined. To obtain a good impedance matching, the impedance of the feeding structure should be matched to the antenna's input impedance. In this antenna, the impedance of the feeding structure is mainly affected by the size of the feeding slot, the feeding cavity, and the probe. Here two main parameters, i.e., the length (L_f) and width (W_f) of the feeding slots, are studied. As can be seen from Fig. 12, both the increasing L_f and W_f can produce a good impedance matching at the desired band.

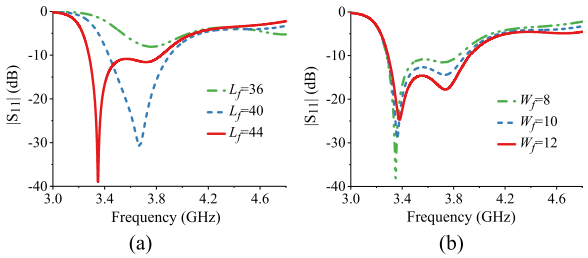

Fig. 12. Impedance matching by the feeding slot. (a) Length L_f. (b) Width W_f.

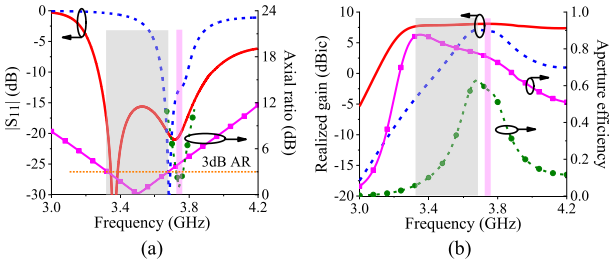

Fig. 13. Comparison of wideband and narrowband slot antennas. (a) $|S_{11}|$ and AR. (b) Realized gain and aperture efficiency. Solid line and solid line with symbol: wideband antenna. Dashed line and dashed line with symbol: narrowband antenna.

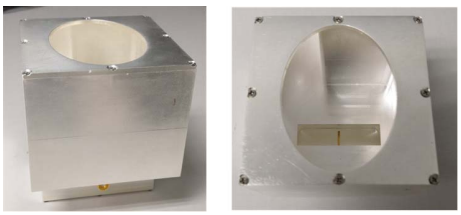

Fig. 14. Photograph of proposed antenna. (a) Full view. (b) Top view. Final dimensions (unit: mm): $a = b = 60$, $c = 50$, $p = 50$, $q = 22$, $s = 20$, $L_x = 44$, $L_y = 57$, $L_t = 22$, $L_f = 45$, $W_f = 12$, $L_p = 16$, $D_p = 9$, $t_1 = t_2 = 2$.

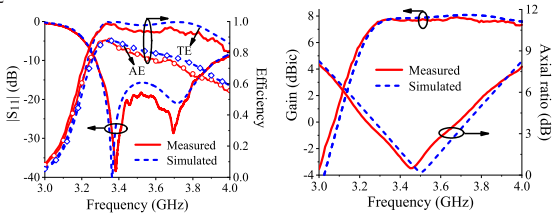

Fig. 15. Measured and simulated results. (a) $|S_{11}|$ and efficiency. (b) Gain and AR. TE: total efficiency; AE: aperture efficiency.

E. Comparison of Wideband and Narrowband Antennas

The comparison of the wideband and narrowband CP slot antennas is shown in Fig. 13. The impedance bandwidth (IBW) and ARBW increased from 2% and 1.0% to 18.7% and 10.3%, respectively. The enhanced bandwidth is obtained without enlarging the antenna size (on the contrary, the electrical size is reduced due to the decreasing

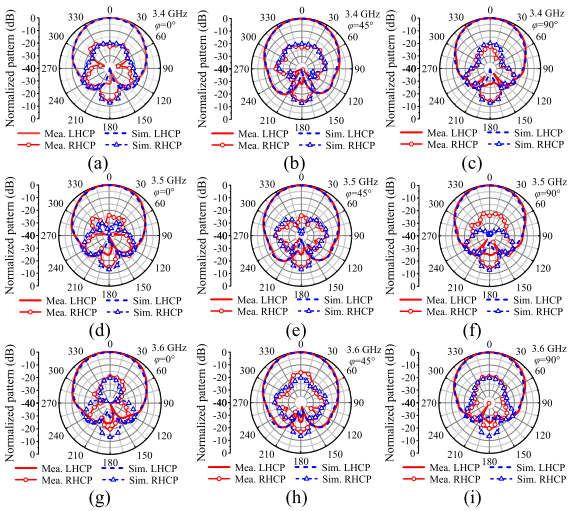

Fig. 16. Measured and simulated radiation patterns at different frequencies. (a)–(c) 3.4 GHz. (d)–(f) 3.5 GHz. (g)–(i) 3.6 GHz.

TABLE II

3 dB AR BEAMWIDTH AT DIFFERENT FREQUENCIES

Planes	3.4 GHz Mea./Sim.	3.5 GHz Mea./Sim.	3.6 GHz Mea./Sim.
XZ-plane ($\varphi = 0°$)	168°/140°	176°/158°	180°/168°
YZ-plane ($\varphi = 90°$)	170°/166°	147°/165°	140°/143°
Diagonal plane ($\varphi = 45°$)	132°/120°	136°/129°	145°/124°

TABLE III

COMPARISON WITH REPORTED CP ANTENNAS

Ref.	Type	Freq. (GHz)	IBW	ARBW (Band)	ARBW (Beam)	TE	AE	Size: mm^3 λ_0^3
[10]	SIW Slot	2.35	3.5%	~1%	N.G.	58%	~20%	93×93×1.58 0.73×0.73×0.02
[11]	SIW Slot	5.72	1.63%	0.44%	~70°	N.G.	54%	40×38×1.5 0.77×0.7×0.03
[14]	Metal cavity Slot	29.9	~6.5%	1.2%	N.G.	97.2%	~84%	60×60×50 1×0.9×0.7
[15]	Metal cavity Slot	3.6	~6.8%	~1%	N.G.	N.G.	N.G.	N.G.
[20]	SIW Slot	5.8	~3%	N.G.	< 70°	N.G.	15.2 dBi	109×109×6.5 2.1×2.1×0.18
[21]	SIW Slot	5.8	3.6%	N.G.	57°	N.G.	88.2%	50×50×3.5 0.97×0.97×0.07
[26]	SIW+Cavity Aperture	60	10.8%	11.6%	>134°	N.G.	~50%	15.2×7.5×6.8 3×1.5×1.35
[27]	Patch	2.27	N.G.	0.9%	>120°	N.G.	~10%	240×240×3 1.8×1.8×0.022
[28]	Patch	2.45	2.7%	0.6%	>140°	N.G.	~10%	200×200×2.5 1.6×1.6×0.02
T.W.	Metal cavity Slot	3.45	18.6%	9.5%	>140°	97%	91%	60×60×50 0.7×0.7×0.58

IBW: Impedance bandwidth; ARBW (Band): Axial-ratio bandwidth; ARBW (Beam): Axial-ratio beamwidth; TE: Total efficiency; AE: Aperture efficiency; T.W. This work; N.G.: Not given. N.A.: Not applicable. The size of the antenna is defined as Length×Width×Height.

operating frequency) or complicating the antenna structure. Besides, the realized gain has a 1 dB increment and the aperture efficiency is increased from 57%–59% to 78%–88%.

III. EXPERIMENTAL RESULTS

After the proposed CP slot antenna is designed, a prototype is fabricated to verify the design concept in experiment. The photograph

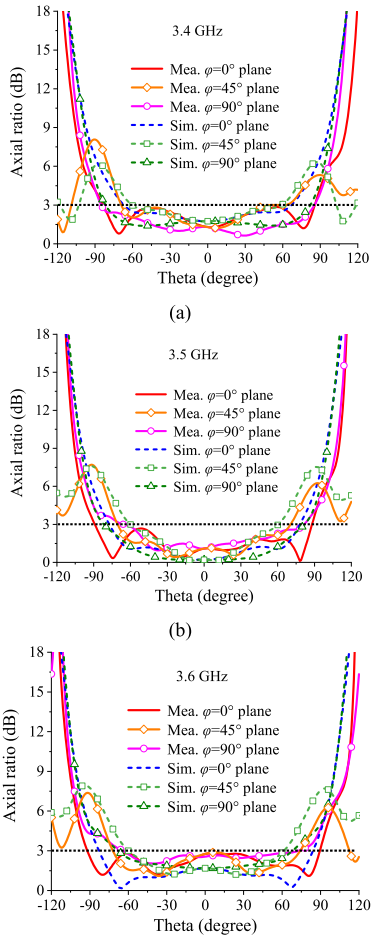

Fig. 17. Measured and simulated AR beamwidth at different frequencies. (a) At 3.4 GHz. (b) At 3.5 GHz. (c) At 3.6 GHz.

of the antenna is given in Fig. 14. Fig. 15 shows the measured and simulated results as a function of frequency. The measured bandwidth is 9.5% at 3.45 GHz (3.29–3.62 GHz), which is a little narrower than the simulated one of 10.3% at 3.5 GHz (3.32–3.68 GHz). This antenna has a flat in-band realized gain of 7.65 dBic ± 0.15 dBic due to the operation of two similar degenerate cavity modes. The measured total efficiency is from 93% to 97%, while the simulated total efficiency is from 98% to 99.5%, both of them demonstrate a very low power loss. The aperture efficiency is higher than 70% with a peak of 91% at 3.3 GHz, while the simulated aperture efficiency is higher than 78%.

The radiation patterns at 3.4, 3.5, and 3.6 GHz at $\varphi = 0°$, $\varphi = 45°$, and $\varphi = 90°$ planes are depicted in Fig. 16, which indicates that the measured copolarization (LHCP) are almost the same as the simulated one, and the measured cross polarization (RHCP) are better than −20 dB. It can also be seen that the copolarizations at these three frequencies are almost the same, which demonstrates a stable radiation pattern over the operating band. The AR beamwidths of the CP slot antenna at three planes are shown in Fig. 17, which indicate that the proposed antenna has a wide AR beamwidth in a wide frequency range. The 3 dB AR beamwidths at 3.4, 3.5, and 3.6 GHz at *xz*-plane and *yz*-plane are all higher than 140°, while the 3 dB AR beamwidths at diagonal planes are higher than 120°. The detailed results of the measured AR beamwidth are provided in Table II.

The comparison with other reported CP slot antennas is provided in Table III. It can be seen that the proposed work has a wide 3 dB ARBW of 9.5%, which is wider than the initial one (Fig. 2) of around 1% and is also wider than the other antennas utilizing degenerate modes [9]–[11], [14], [15], [22]–[24], [27], [28]. The improvement in ARBW is achieved without introducing extra feeding network or coupling structure and without enlarging the antenna's size. The AR beamwidth is compared at two principal planes, i.e., *xz*-plane and *yz*-plane, as most of the CP antennas only gave the AR beamwidth at these two planes. It can be further seen that the proposed antenna also exhibits its attractive merit of 140° 3 dB AR beamwidth in a wide frequency range while the AR beamwidths of other CP CBSAs [11], [20], [21] were less than 70°. The work [26] was a cavity-backed aperture antenna. It had similar ARBW and AR beamwidth compared to the proposed work. However, its AR beamwidth was only given at the center frequency. Two CP patch antennas with wide AR beamwidth are also provided in the table, demonstrating that the proposed CP slot antenna has comparable AR beamwidth. The proposed antenna has a full-metal structure to achieve a high power-handling capacity and a high efficiency, although it is bulky.

IV. Conclusion

This communication presents a novel design of a wide-bandwidth and wide-ARbeamwidth CP CBSA. The triangular prisms are introduced and utilized to produce two degenerate cavity modes TE_{101} and TE_{011} toward the CP radiation. By properly modifying the sizes of the prisms and radiation slot, the proposed CP slot antenna is then demonstrated to achieve a wide ARBW of about 10.3% based on a single pair of degenerate modes, which is wider than the initial one of 1%. The proposed work brings in the new perspective that the degenerate modes can also be employed to obtain a wide ARBW without introducing extra wideband feeding network or coupling structures. The single resonant cavity and cavity-backed antenna structure is well exhibited to have its capability in simultaneous achievement of a wide AR beamwidth and an enhanced ARBW. Finally, an antenna prototype is fabricated and tested to illustrate that the measured AR beamwidth exceeds 140° with an ARBW of 9.5%. In addition, the proposed CP slot antenna also owns a few attractive features, including high radiation efficiency, high aperture efficiency, stable realized gain, and stable radiation pattern.

References

[1] Z. Zhang, X. Cao, J. Gao, S. Li, and J. Han, "Broadband SIW cavity-backed slot antenna for endfire applications," *IEEE Antennas Wireless Propag. Lett.*, vol. 17, no. 7, pp. 1271–1275, Jul. 2018.

[2] S. Liao, P. P. Chen Wu, K. M. Shum, and Q. Xue, "Substrate-integrated waveguide-based 60-GHz resonant slotted waveguide arrays with wide impedance bandwidth and high gain," *IEEE Trans. Antennas Propag.*, vol. 63, no. 7, pp. 2922–2931, Jul. 2015.

[3] W. Li, K. D. Xu, X. Tang, Y. Yang, Y. Liu, and Q. H. Liu, "Substrate integrated waveguide cavity-backed slot array antenna using high-order radiation modes for dual-band applications in *K*-band," *IEEE Trans. Antennas Propag.*, vol. 65, no. 9, pp. 4556–4565, Sep. 2017.

[4] Y. Xiaole, N. Daning, L. Shaodong, L. Zhengjun, and W. Wutu, "Design of a wideband waveguide slot array antenna and its decoupling method for synthetic aperture radar," in *Proc. 38th Eur. Microw. Conf.*, Oct. 2008, pp. 135–138.

[5] Y.-M. Wu, S.-W. Wong, H. Wong, and F.-C. Chen, "A design of bandwidth-enhanced cavity-backed slot filtenna using resonance windows," *IEEE Trans. Antennas Propag.*, vol. 67, no. 3, pp. 1926–1930, Mar. 2019.

[6] W. Yuan, X. Liang, L. Zhang, J. Geng, W. Zhu, and R. Jin, "Rectangular grating waveguide slot array antenna for SATCOM applications," *IEEE Trans. Antennas Propag.*, vol. 67, no. 6, pp. 3869–3880, Jun. 2019.

[7] R.-S. Chen *et al.*, "High-efficiency and wideband dual-resonance full-metal cavity-backed slot antenna array," *IEEE Antennas Wireless Propag. Lett.*, vol. 19, no. 8, pp. 1360–1364, Aug. 2020.

[8] R.-S. Chen *et al.*, "High-isolation in-band full-duplex cavity-backed slot antennas in a single resonant cavity," *IEEE Trans. Antennas Propag.*, early access, Oct. 27, 2020, doi: 10.1109/TAP.2020.3032846.

[9] G. Q. Luo, Z. F. Hu, Y. Liang, L. Y. Yu, and L. L. Sun, "Development of low profile cavity backed crossed slot antennas for planar integration," *IEEE Trans. Antennas Propag.*, vol. 57, no. 10, pp. 2972–2979, Oct. 2009.

[10] L. Ge, Y. Li, J. Wang, and C.-Y.-D. Sim, "A low-profile reconfigurable cavity-backed slot antenna with frequency, polarization, and radiation pattern agility," *IEEE Trans. Antennas Propag.*, vol. 65, no. 5, pp. 2182–2189, May 2017.

[11] Y. Xu, Z. Wang, and Y. Dong, "Circularly polarized slot antennas with dual-mode elliptic cavity," *IEEE Antennas Wireless Propag. Lett.*, vol. 19, no. 4, pp. 715–719, Apr. 2020.

[12] Y. Lang, S.-W. Qu, and J.-X. Chen, "Wideband circularly polarized substrate integrated cavity-backed antenna array," *IEEE Antennas Wireless Propag. Lett.*, vol. 13, pp. 1513–1516, 2014.

[13] D.-F. Guan, C. Ding, Z.-P. Qian, Y.-S. Zhang, Y. Jay Guo, and K. Gong, "Broadband high-gain SIW cavity-backed circular-polarized array antenna," *IEEE Trans. Antennas Propag.*, vol. 64, no. 4, pp. 1493–1497, Apr. 2016.

[14] X. Wu, F. Yang, F. Xu, and J. Zhou, "Circularly polarized waveguide antenna with dual pairs of radiation slots at Ka-band," *IEEE Antennas Wireless Propag. Lett.*, vol. 16, pp. 2947–2950, 2017.

[15] Y.-M. Wu, S.-W. Wong, J.-Y. Lin, L. Zhu, Y. He, and F.-C. Chen, "A circularly polarized cavity-backed slot antenna with enhanced radiation gain," *IEEE Antennas Wireless Propag. Lett.*, vol. 17, no. 6, pp. 1010–1014, Jun. 2018.

[16] J. Wu, Y. J. Cheng, H. B. Wang, Y. C. Zhong, D. Ma, and Y. Fan, "A wideband dual circularly polarized full-corporate waveguide array antenna fed by triple-resonant cavities," *IEEE Trans. Antennas Propag.*, vol. 65, no. 4, pp. 2135–2139, Apr. 2017.

[17] S.-G. Zhou, G.-L. Huang, and T.-H. Chio, "A lightweight, wideband, dual-circular-polarized waveguide cavity array designed with direct metal laser sintering considerations," *IEEE Trans. Antennas Propag.*, vol. 66, no. 2, pp. 675–682, Feb. 2018.

[18] M. Akbari, A. Farahbakhsh, and A.-R. Sebak, "Ridge gap waveguide multilevel sequential feeding network for high-gain circularly polarized array antenna," *IEEE Trans. Antennas Propag.*, vol. 67, no. 1, pp. 251–259, Jan. 2019.

[19] J. Wu, C. Wang, and Y. Guo, "A wideband circularly polarized array antenna with compact and high-efficiency feeding network," *IEEE Trans. Antennas Propag.*, vol. 68, no. 1, pp. 62–69, Jan. 2020.

[20] W. Han, F. Yang, R. Long, L. Zhou, and F. Yan, "Single-fed low-profile high-gain circularly polarized slotted cavity antenna using a high-order mode," *IEEE Antennas Wireless Propag. Lett.*, vol. 15, pp. 110–113, 2016.

[21] W. Yang, S. Chen, W. Che, Q. Xue, and Q. Meng, "Compact high-gain metasurface antenna arrays based on higher-mode SIW cavities," *IEEE Trans. Antennas Propag.*, vol. 66, no. 9, pp. 4918–4923, Sep. 2018.

[22] X. Fang, K. W. Leung, and E. H. Lim, "Singly-fed dual-band circularly polarized dielectric resonator antenna," *IEEE Antennas Wireless Propag. Lett.*, vol. 13, pp. 995–998, 2014.

[23] H. San Ngan, X. S. Fang, and K. W. Leung, "Design of dual-band circularly polarized dielectric resonator antenna using a higher-order mode," in *Proc. IEEE-APS Top. Conf. Antennas Propag. Wireless Commun. (APWC)*, Sep. 2012, pp. 424–427.

[24] S. Gotra, G. Varshney, R. S. Yaduvanshi, and V. S. Pandey, "Dual-band circular polarisation generation technique with the miniaturisation of a rectangular dielectric resonator antenna," *IET Microw., Antennas Propag.*, vol. 13, no. 10, pp. 1742–1748, 2019.

[25] C. A. Balanis, *Antenna Theory: Analysis and Design*. Hoboken, NJ, USA: Wiley, 2016.

[26] X. Bai, S.-W. Qu, S. Yang, J. Hu, and Z.-P. Nie, "Millimeter-wave circularly polarized tapered-elliptical cavity antenna with wide axial-ratio beamwidth," *IEEE Trans. Antennas Propag.*, vol. 64, no. 2, pp. 811–814, Feb. 2016.

[27] N.-W. Liu, L. Zhu, and W.-W. Choi, "Low-profile wide-beamwidth circularly-polarised patch antenna on a suspended substrate," *IET Microw., Antennas Propag.*, vol. 10, no. 8, pp. 885–890, May 2016.

[28] X. Zhang, L. Zhu, and N.-W. Liu, "Pin-loaded circularly-polarized patch antennas with wide 3-dB axial ratio beamwidth," *IEEE Trans. Antennas Propag.*, vol. 65, no. 2, pp. 521–528, Feb. 2017.